Multiple scattering in the Compton effect. Relativistic cross section for double scattering

Vesa Halonen
Department of Physics, University of Helsinki, Helsinki, Finland

Brian Williams
Department of Applied Physics, University of Strathclyde, Glasgow, Scotland

(Received 28 December 1977)

The angular distributions of double scattering for aluminum and nickel have been studied using the relativistic Klein-Nishina cross section. The differences between the nonrelativistic Thomson cross section and the Klein-Nishina cross section are studied at different energies. The effects of using a momentum-dependent (Ribberfors) cross section are studied. It is found that the Ribberfors cross section can be replaced by the Klein-Nishina cross section in most cases of interest in double scattering. The results are applied to experimental Compton profiles of aluminum and nickel measured at Am and Te energies. The corrected profiles are found to be independent of sample thickness and/or incident energy, within the statistical errors.

I. INTRODUCTION

It is now widely accepted that multiple-scattering events may give rise to significant systematic errors in measured Compton profiles.[1] Procedures for correcting for multiple scattering have been discussed by several authors.[2-8] In this paper we present an extended version of the Monte Carlo solution of multiple scattering discussed in our previous papers.[2-4] We have studied the differences between relativistic and nonrelativistic cross sections for double scattering at different energies and scattering angles as well as the effects of the momentum-dependent terms in the single-scattering cross section on the intensities and spectral distributions of double scattering.

The relationship of the relativistic Compton cross section to the momentum distribution of bound electrons has been derived by Ribberfors.[9,10] In the case of stationary electrons, his formula reduces to the relativistic Klein-Nishina cross section. Ribberfors[10] has recently argued that in multiple-scattering calculations the momentum-dependent cross sections for scattering should be used instead of the Klein-Nishina cross section for scattering from stationary electrons. In this paper an expression for the double-scattering cross section is derived from the Ribberfors cross section and the resulting intensity and angular distribution are examined.

Three alternative Monte Carlo techniques[3,5,8] have been used to calculate the effects of multiple scattering in Compton-profile measurements. All of them are fairly time consuming, but an effective use of variation-reduction techniques[3,8] allows great savings of computing time. A further great reduction of computing time is obtained by calculating separately the intensity and the spectral distribution of double scattering. In our earlier paper[3] we showed that only 100 double-scattering events are needed to obtain a spectral distribution of sufficient accuracy, while 10 000 double-scattering events had to be generated to obtain ~1% accuracy in the ratio of double-to-single scattering.

In this paper the new Monte Carlo calculations are applied to aluminum and nickel at different energies. The angular distributions of double scattering are given in reflection geometry. Only the total double scattering is studied, although the method allows a separate study of the elastic and inelastic scattering. As a final check of the validity of the calculations the procedure is applied to the Compton profiles of aluminum and nickel measured from samples of different thicknesses. Experimental profiles for various ionic crystals have also been corrected for double scattering and are published elsewhere.[1,11]

II. THEORETICAL

A. Inelastic (Compton) scattering

The basic features of the Monte Carlo technique have been described in detail in previous papers.[2,3] The sample configuration is a cylinder (radius A) situated in the three-dimensional xyz system so that the surface planes of the cylinder are perpendicular to the z axis at $z=0$ and $z=d$. We use the reflection geometry in which the incident and detected rays make angles ψ_1 and ψ_2, respectively, with the specimen surface. If J_0 is the flux of the incident photons, the flux of Compton scattered photons is

$$J_{1C}=J_0\int_{\mathrm{Vol}}\exp\left(-\frac{\mu z_1}{\sin\psi_1}-\frac{\mu(C)z_1}{\sin\psi_2}\right)\rho\,dV_1\left(\frac{d\sigma}{d\Omega}\right)_C d\Omega\,, \quad (1)$$

where $d\Omega$ is the solid angle subtended by the detector and ρ is the atomic density. μ and $\mu(C)$ are

the linear attenuation coefficients for the incident and scattered radiation, respectively, and $z_1/\sin\psi_1$ and $z_1/\sin\psi_2$ describe the path of the photon in the sample. $(d\sigma/d\Omega)_C$ is the Compton-scattering cross section per atom. It can be given either in the impulse approximation (IA) or in the Waller-Hartree (WH) theory. In IA,

$$\left(\frac{d\sigma}{d\Omega}\right)_C = \sum_{j=1}^{N} \int_0^{\epsilon_j} n_j C(\omega') J_j(p_z)\, d\omega' , \tag{2}$$

where N is the number of one electron orbitals and n_j is the number of electrons in each orbital. Electron binding energies E_{Bj} of each orbital are taken into account by integrating the Compton profiles of each orbital up to the binding energy cutoff; i.e.,

$$E_{Bj} = \omega - \epsilon_j . \tag{3}$$

$J_j(p_z)$ is the one-dimensional Compton profile of each orbital and it is normalized,

$$\int_{-\infty}^{\infty} J_j(p_z)\, dp_z = 1 . \tag{4}$$

$C(\omega')$ describes the energy and the angular dependence of the cross section and is given approximately by

$$C(\omega') = \frac{1}{2}\frac{\omega'}{\omega}\frac{mr_0^2}{|\vec{k}|}\left[\left(\frac{R}{R'}+\frac{R'}{R}\right) - 2\cos^2\xi\right], \tag{5}$$

where ω and ω' are the initial and final photon energies, respectively, $r_0 = e^2/mc^2$ is the classical electron radius, ξ is the angle between the electric vector of the incident photon and the direction of the scattered photon, and $\vec{k}$ is the x-ray scattering vector or

$$|\vec{k}| = (\omega^2 + \omega'^2 - 2\omega\omega'\cos\theta)^{1/2} . \tag{6}$$

θ is the scattering angle for single scattering. R and R' in Eq. (5) are defined by Ribberfors and they include the momentum-dependent terms in the cross section.

In WH we obtain

$$\left(\frac{d\sigma}{d\Omega}\right)_C = \frac{r_0^2}{2}\left(\frac{\omega_0'}{\omega}\right)^2\left(\frac{\omega}{\omega_0'}+\frac{\omega_0'}{\omega} - 2\cos^2\xi\right) f_C , \tag{7}$$

where f_C is the incoherent scattering factor per atom. The subscript 0 on ω' refers to the electron at rest.

B. Elastic (Rayleigh) scattering

The usual range of energies in Compton-profile experiments is about 10–160 keV. The scattering cross section in the classical Thomson form is

$$\left(\frac{d\sigma}{d\Omega}\right)_R = r_0^2 \sin^2\xi f_R^2 , \tag{8}$$

where f_R is the free-atom scattering factor. The flux of the elastically scattered photons is obtained from Eq. (1) by replacing the Compton cross section by the Rayleigh cross section and setting $\mu(C) = \mu(R) = \mu$.

All the above expressions are for polarized incident radiation. For unpolarized incident radiation the average over the polarization of the incoming photon gives

$$\sin^2\xi \doteq \tfrac{1}{2}(1+\cos^2\theta) . \tag{9}$$

In order to obtain the total flux of the photons we sum the expressions for elastic and inelastic scattering.

C. Total double scattering

In previous papers the formulas for double scattering were written in the nonrelativistic limit using the Thomson cross section for scattering. In the following treatment we will use the relativistic Compton cross section of Eq. (2) for inelastic scattering events. The flux of photons scattered twice into a solid angle $d\Omega$ is

$$J_2 = J_0\left[\sum_{I,J}\int\!\!\int_{\text{Vol}} e^{-\mu z_1/\sin\psi_1}\frac{1}{r_1^2}e^{-\mu(I)r_1}\left(\frac{d\sigma}{d\Omega}\right)_{1I} \times e^{-\mu(J)z_2/\sin\psi_2}\left(\frac{d\sigma}{d\Omega}\right)_{2J}\rho dV_1\,\rho dV_2\right]d\Omega , \tag{10}$$

where we must sum over all possible scattering processes (I, J mean Compton or Rayleigh scattering). ρdV_1 and ρdV_2 give the number of atoms around the first and second collision points in the volume elements dV_1 and dV_2, respectively. μ, $\mu(I)$, and $\mu(J)$ are the linear absorption coefficients for primary, intermediate, and exit radiation and $z_1/\sin\psi_1$, r_1 and $z_2/\sin\psi_2$ are the corresponding paths of the photons. The scattering cross sections $(d\sigma/d\Omega)_{1J}$ and $(d\sigma/d\Omega)_{2J}$ are obtained from Eqs. (2)–(8) for each scattering event.

In order to derive the spectral distribution of double scattering we use the following expressions:

$$\int_{E_1} I_{1C}(E_1)\, dE_1 = \frac{1}{2}\sum_{j=1}^{N} n_j \int_0^{\epsilon_j'} \frac{\omega'}{\omega}\frac{mcr_0^2}{(\omega^2+\omega'^2-2\omega\omega'\cos\theta_1)^{1/2}} \times J_j(p_z)\, d\omega' , \tag{11}$$

$$\int_{E_2} I_{2C}(E_2)\, dE_2 = \frac{1}{2}\sum_{j=1}^{N} n_j \int_0^{\epsilon_j''} \frac{\omega''}{\omega'}\frac{mcr_0^2}{(\omega'^2+\omega''^2-2\omega'\omega''\cos\theta_2)^{1/2}} \times J_j(p_z)\, d\omega'' ,$$

where θ_1 and θ_2 are the scattering angles for the first and second collisions, respectively. ϵ_j' and ϵ_j'' are determined from Eq. (3) for each orbital and ω'' is the final energy of the photons after two collisions. We also write

$$B_1 = R/R' + R'/R - 2,$$
$$B_2 = R'/R'' + R''/R' - 2. \tag{12}$$

Then, integrating over the sample, Eq. (10) becomes

$$J_2(E)dE = J_0\rho^2\Bigg(\sum_{I,J}\int_0^d\int_0^\infty\int_0^\pi\int_0^{2\pi} e^{-\mu z_1/\sin\psi_1}\delta(r_1,\alpha,\phi)\int_{E_1} e^{-\mu(I)r_1}(B_1 - 2\sin^2\xi_1)I_{1I}(E_1)e^{-\mu(J)z_2/\sin\psi_2}$$
$$\times (B_2 - 2\sin^2\xi_2)I_{2J}(E-E_1)dE_1 A\,dz_1\,dr_1$$
$$\times \sin\alpha\,d\alpha\,d\phi\Bigg)dE\,d\Omega, \tag{13}$$

where the δ function is 1 if the second collision point is inside the sample and 0 if it is outside the sample. In Eq. (13) we have summed over all directions of polarization of the photons after first and second collisions. E_1 and E_2 describe the energy shifts for each scattering event and since E is the total shift in energy

$$E = E_1 + E_2. \tag{14}$$

$r_1^2 dr_1 \sin\alpha\,d\alpha d\phi$ is the volume element of the second scattering in the spherical coordinate system. In Eq. (13), we can write for elastic events:

$$I_{1R} = \tfrac{1}{2}f_R^2, \quad B_1 = 0, \tag{15}$$

with corresponding expressions for the second elastic scattering. In order to solve Eq. (13) for incident unpolarized radiation we illustrate the situation with the aid of Fig. 1. Using the rules of spherical triangles we obtain

$$\cos\theta_2 = \cos\theta\cos\theta_1 + \sin\theta\sin\theta_1\cos(\phi - \phi_1). \tag{16}$$

The observation that the direction of twice-scattered photons must be the same as the direction of single-scattered photons gives

$$\cos\xi = \cos\theta_2\cos\xi_1 + \sin\xi_1\sin\xi_2. \tag{17}$$

We now resolve the incident radiation into two orthogonally polarized components, each carrying one-half of the incident intensity, parallel ($\phi = 0$) and perpendicular ($\phi = 90°$) to the single-scattering plane. Then we obtain, after lengthy calculations,

$$J_2(E)\,dE = J_0\rho^2\Bigg\{\sum_{I,J}\int_0^d\int_0^\infty\int_0^\pi\int_0^{2\pi} e^{-\mu z_1/\sin\psi_1}\delta(r_1,\alpha,\phi)$$
$$\times\Bigg(\int_{E_1} B_1 e^{-\mu(I)r_1}I_{1I}(E_1)B_2 e^{-\mu(J)z_2/\sin\psi_2}I_{2J}(E-E_1)\,dE_1$$
$$+\int_{E_1}(2-D)e^{-\mu(I)r_1}B_1 I_{1I}(E_1)e^{-\mu(J)z_2/\sin\psi_2}I_{2J}(E-E_1)\,dE_1$$
$$+\int_{E_1}(1+\cos^2\theta_1)e^{-\mu(I)r_1}I_{1I}(E_1)B_2 e^{-\mu(J)z_2/\sin\psi_2}I_{2J}(E-E_1)\,dE_1$$
$$+\int_{E_1} 4P(\theta,\theta_1,\theta_2)e^{-\mu(I)r_1}I_{1I}(E_1)e^{-\mu(J)z_2/\sin\psi_2}I_{2J}(E-E_1)\,dE_1\Bigg)$$
$$\times A\,dz_1\,dr_1\sin\alpha\,d\alpha\,d\phi\Bigg\}dE\,d\Omega, \tag{18}$$

where

$$D = \frac{[\sin^2\theta - (\cos\theta_2 - \cos\theta\cos\theta_1)\cos\theta_2]^2}{\sin^2\theta - (\cos\theta_2 - \cos\theta\cos\theta_1)^2} + \frac{[\sin^2\theta_1\sin^2\theta - (\cos\theta_2 - \cos\theta\cos\theta_1)^2]\cos^2\theta_2}{\sin^2\theta\cos^2\theta_1 + (\cos\theta_2 - \cos\theta_1\cos\theta)^2}, \tag{19}$$

and $P(\theta,\theta_1,\theta_2)$ gives the angular dependence of the Thomson cross section for double scattering, where

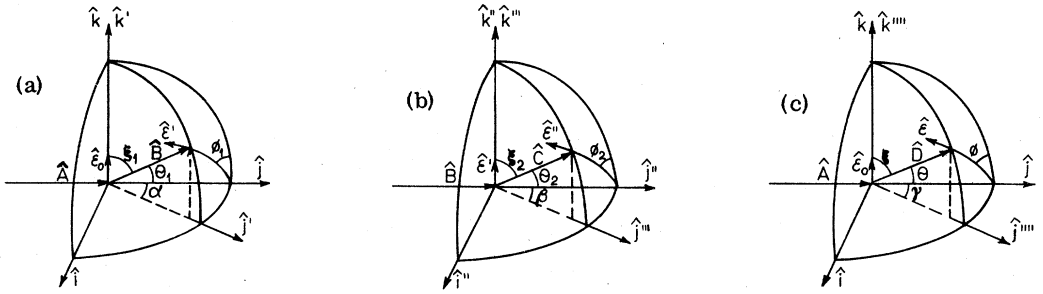

FIG. 1. Description of the interaction for a pair of events of double scattering [(a) and (b)]. (c) describes the single scattering. $\hat{\epsilon}_0$ is the electric vector of the incident photon and $\hat{\epsilon}$, $\hat{\epsilon}'$, and $\hat{\epsilon}''$ are the electric vectors of the scattered photons in each case. $\hat{A}$ is the direction of the incoming photon, $=\hat{j}$; $\hat{B}$ is the direction of the first scattered photon, $=\sin\xi_1\hat{j}'+\cos\xi_1\hat{k}=\hat{j}''$; $\hat{C}$ is the direction of the second scattered photon, $=\sin\xi_2\hat{j}''''+\cos\xi_2\hat{k}''''=\hat{D}$; $\hat{D}$ is the direction of the single scattering photon, $=\sin\xi\hat{j}''''+\cos\xi\hat{k}''''=\hat{C}$.

$$P(\theta,\theta_1,\theta_2)=\tfrac{1}{2}(\cos^2\theta+\cos^2\theta_1+\cos^2\theta_2-2\cos\theta\cos\theta_1\cos\theta_2+\cos^2\theta_1\cos^2\theta_2). \quad (20)$$

The first three terms in large parentheses of Eq. (18) could be called the Ribberfors correction; the last term is the classical term.

In the case of stationary electrons we replace $I_{1C}(E_1)$ and $I_{2C}(E_2)$ in Eq. (18) by the corresponding quantities from the Waller-Hartree theory [Eq. (7)] to obtain

$$J_2=J_0r_0^2\left(\frac{\omega_0''}{\omega}\right)^2\rho^2\Bigg(\sum_{I,J}\int_0^d\int_0^\infty\int_0^\pi\int_0^{2\pi}e^{-\mu z_1/\sin\psi_1}\delta(r_1,\alpha,\phi)e^{-\mu(f)r_1}I_{1I}\,e^{-\mu(f)z_2/\sin\psi_2}I_{2J}$$

$$\times[B_1B_2+(2-D)B_1+(1+\cos^2\theta_1)B_2+4P(\theta,\theta_1,\theta_2)]A\,dz_1\,dr_1\sin\alpha\,d\alpha\,d\phi\Bigg)d\Omega, \quad (21)$$

where D is given in Eq. (19) and

$$B_1=\frac{\omega}{\omega_0'}+\frac{\omega_0'}{\omega}-2,\quad B_2=\frac{\omega_0'}{\omega_0''}+\frac{\omega_0''}{\omega_0'}-2. \quad (22)$$

I_{1I} and I_{2J} are either $\frac{1}{2}f_C$ or $\frac{1}{2}f_R^2$ depending on the nature of the scattering. Equation (21) includes our previous classical Thomson result as a limiting case. When $\omega\simeq\omega_0'\simeq\omega_0''$ and also $f_R^2+f_c\simeq Z$ (the number of electrons per atom) we arrive at exactly the same expression as in our earlier paper.

D. Correction for double scattering

Let $J_E(E)$ be the experimental Compton profile before the energy-dependent corrections of absorption and cross section have been applied:

$$J_E(E)=C(E)A(E)J_E(p_z), \quad (23)$$

where the energy dependence of $C(E)$ is given in Eq. (5) combined with Eq. (9) and the absorption term $A(E)$ has been written in Eq. (1). $J_E(p_z)$ is the experimental Compton profile on a momentum scale. Let $J(E)$ be the true single-scattered profile which we wish to obtain.

If we fix the normalization so that

$$\int_E J_E(E)\,dE=\int_E J(E)\,dE=\int_E J_2(E)\,dE=N, \quad (24)$$

we obtain, for $J(E)$,

$$J(E)=(N+\lambda)J_E(E)-\lambda J_2(E), \quad (25)$$

where λ is the ratio of double-to-single scattering. N is usually chosen so that it is equal to the area of the theoretical single profile in a chosen range of energy. Finally, in order to obtain the measured Compton profile on a momentum scale, we must apply Eq. (23) to $J(E)$.

III. RESULTS AND DISCUSSION

A. Relativistic Klein-Nishina and nonrelativistic Thomson cross sections of double scattering

The ratio of double-to-single scattering as a function of scattering angle for aluminum is given in Fig. 2. The photon energies are those most often used in experimental work, viz., 159.0 keV (Te), 59.537 keV (Am) and 17.4 keV (Mo$K\alpha$). For each calculation infinite-thickness sample geometry was used. This assumes that the optical thickness of the sample $\mu d>2.0$.[14] In order to show the differences between the relativistic and nonrela-

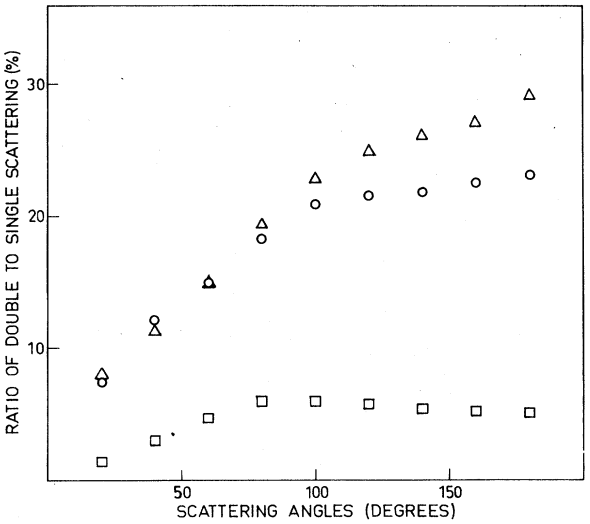

FIG. 2. Angular distribution of double scattering for aluminum with the optical thickness $\mu d > 2.0$, □, ○, Δ refer to Mo $K\alpha$, Am, and Te energies, respectively. The radius of the cylindrical sample was 0.6 cm. For each point 10 000 single- and double-scattering events were generated within the sample.

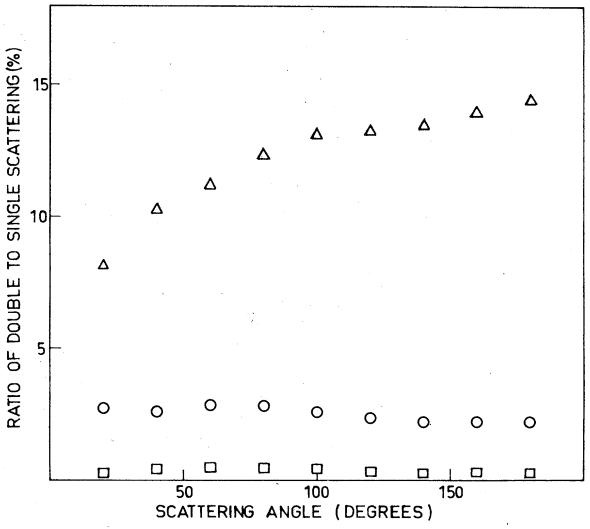

FIG. 3. Angular distribution of double scattering for nickel with the optical thickness $\mu d = 0.1$ (cf. notation in Fig. 2).

tivistic intensities we have given the Klein-Nishina and Thomson results in Table I. It is seen that at Am energy the results of the two cross sections are almost indistinguishable. This will also be true for energies lower than Am energy, because the quantity $(\omega_0'/\omega + \omega/\omega_0')$ approaches the value of 2 and Eq. (21) reduces to the nonrelativistic case. For higher energies, the differences become more significant and indeed, if the photon energy is 160 keV or higher, the relativistic treatment is necessary.

In the results of Fig. 2 the infinite sample geometry was employed. In order to study the combined effect of sample geometry and the different cross sections we present the angular distributions of double scattering for nickel at the same energies as above, but with optical thickness $\mu d = 0.1$. The ratios have been plotted in Fig. 3. It can be seen that for thin samples, there is a trend away from any angular dependence. This result implies that for sufficiently thin samples the geometry becomes more important than the form of the cross section in determining the intensity of double scattering. In Table II we compare the total intensities of double scattering calculated with the Thomson and Klein-Nishina formulas. Use of the Klein-Nishina cross section now makes less difference than for optically thicker samples. This was expected because the probability of obtaining a given pair of scat-

TABLE I. Single and double scattering in aluminum for Am and Te radiation. The sample thicknesses were effectively infinite; i.e., $\mu d > 2.0$. The Thompson and Klein-Nishina (KN) double scattering as well as single scattering are given in electron units. The values of f_R and f_C have been tabulated elsewhere (Refs. 12 and 13).

	^{241}Am radiation			Te radiation		
θ	Single $f_R^2 + f_C$	Double Thomson	Double KN	Single $f_c^2 + f_c$	Double Thomson	Double KN
60	13.360	1.987	1.999	13.000	1.839	1.944
80	12.250	2.411	2.425	13.000	2.443	2.541
100	13.150	2.733	2.736	13.000	2.938	2.973
120	13.090	2.822	2.815	13.000	3.254	3.236
140	13.070	2.863	2.851	13.000	3.430	3.393
160	13.050	2.957	2.943	13.000	3.581	3.539
180	13.070	3.003	3.012	13.000	3.724	3.835

TABLE II. Single and double scattering in nickel for Am and Te radiation. The sample thicknesses were chosen so that $\mu d = 0.1$. The units are the same as in Table I.

	^{241}Am radiation			Te radiation		
θ	Single $f_R^2 + f_c$	Double Thomson	Double KN	Single $f_R^2 + f_c$	Double Thomson	Double KN
60	32.880	0.931	0.930	28.300	3.083	3.183
80	29.320	0.829	0.827	28.190	3.406	3.480
100	28.690	0.735	0.732	28.030	3.669	3.668
120	28.400	0.660	0.655	28.000	3.743	3.696
170	28.360	0.625	0.621	28.000	3.832	3.762
160	28.350	0.621	0.617	28.000	3.966	3.894
180	28.340	0.624	0.622	28.000	3.978	4.018

tering angles is highly restricted by the sample geometry and the differences arise from the asymmetric nature of the Klein-Nishina formula.

B. Relativistic Klein-Nishina and Ribberfors cross sections

In order to study the validity of using the Klein-Nishina formula for double scattering it did not appear feasible to compare Eqs. (18) and (21) for double scattering. Rather, by examining the single scattering at different angles and energies we can deduce from those results the differences between the two cross sections, Eqs. (2) and (7). Figure 4 gives the results of the calculations as a function of scattering angle at Am and Mo $K\alpha$ energies for aluminum and nickel. For Am the two results are in agreement within 2%, if the scattering angle is higher than 20°. In γ-ray Compton measurements the sample geometry is usually limited by the absorption or the geometrical thickness so that the probability of obtaining such a small scattering angle in double scattering is very small. At Mo $K\alpha$ energies, the differences between the two cross sections are more prominent and especially, at small scattering angles, the calculations based on the Ribberfors and/or Klein-Nishina cross sections make a significant difference. These findings suggest that at the energies higher than 60 keV, or even at smaller energies and high scattering angles, one can use

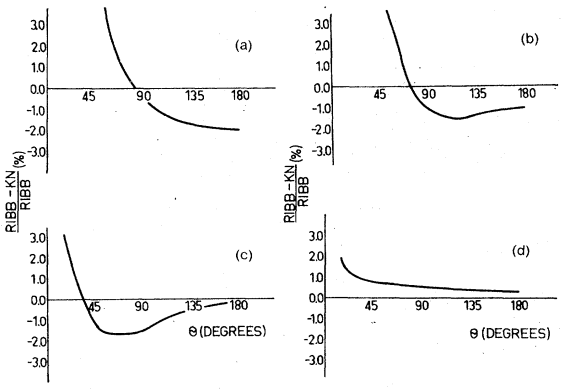

FIG. 4. Differences between the relativistic Klein-Nishina and Ribberfors cross sections for nickel and aluminum, (a) and (b) are at Mo $K\alpha$ energy in the case of nickel and aluminum, respectively, and (c) and (d) are the corresponding results at Am energy.

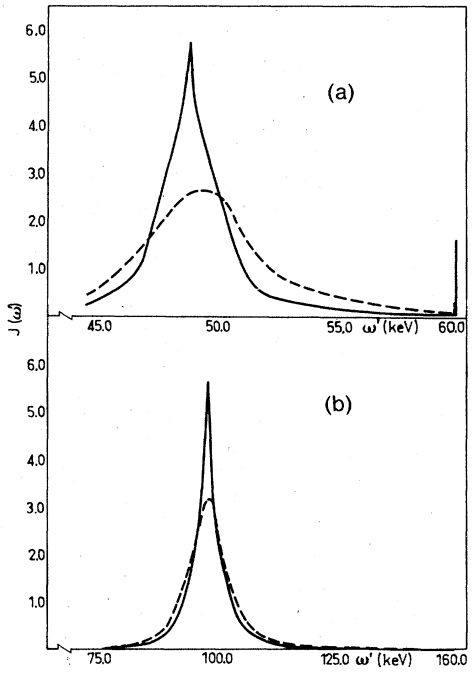

FIG. 5. Spectral distributions of double scattering for nickel at Am (a) and Te energies (b) with the corresponding single profiles. Elastic and double-elastic lines are also indicated. The ratio of the widths of the double profile to the width of the single profile is ~ 2.2 in both cases.

TABLE III. Compton profiles of aluminum. The measured profiles are given before and after correcting for double scattering. The area from 0 to 7 a.u. is 6.16 electrons.

p_z	Theory[a]	Theory[b]	No correction for MS 0.1 cm	No correction for MS 0.01 cm	Corrected for MS 0.1cm	Corrected for MS 0.01cm
0.0	3.985	4.005	3.953 ± 0.9%	4.032 ± 1.4%	4.064 ± 0.9%	4.058 ± 1.4%
0.1	3.996	3.983	3.925	4.001	4.035	4.027
0.2	3.944	3.888	3.828	3.905	3.933	3.929
0.3	3.805	3.752	3.665	3.741	3.762	3.764
0.4	3.611	3.570	3.444	3.519	3.530	3.539
0.5	3.356	3.322	3.177	3.249	3.251	3.267
0.6	3.036	3.013	2.881	2.948	2.941	3.963
0.7	2.652	2.637	2.577	2.634	2.622	2.646
0.8	2.207	2.225	2.286	2.327	2.319	2.336
0.9	1.767	1.792	2.020	2.048	2.042	2.054
1.0	1.653	1.574	1.789 ± 1.4%	1.807 ± 2.1%	1.800 ± 1.4%	1.816 ± 2.1%
1.2	1.513	1.471	1.459	1.451	1.454	1.451
1.4	1.385	1.361	1.289	1.261	1.277	1.259
1.6	1.256	1.244	1.211	1.183	1.197	1.186
1.8	1.134	1.127	1.136	1.132	1.120	1.129
2.0	1.023	1.014	1.034	1.044	1.015	1.041
2.2	0.920	0.906	0.928	0.927	0.907	0.923
2.4	0.815	0.809	0.820	0.808	0.791	0.803
2.6	0.715		0.728	0.706	0.706	0.700
2.8	0.640		0.656	0.636	0.635	0.631
3.0	0.569		0.587 ± 2.4%	0.572 ± 3.0%	0.568 ± 2.4%	0.566 ± 3.0%
3.5	0.424		0.440	0.425	0.425	0.421
4.0	0.322		0.336	0.313	0.323	0.310
4.5	0.245		0.259	0.247	0.248	0.245
5.0	0.200		0.205	0.201	0.197	0.199
6.0			0.141	0.130	0.135	0.129
7.0			0.095 ± 5.5%	0.101 ± 3.3%	0.091 ± 5.5%	0.100 ± 3.3%

[a]Reference 15. [b]Reference 16.

either of the cross sections to calculate the intensity of double or single scattering without any significant difference in the final result.

C. Experimental Compton profiles of aluminum and nickel after correcting for double scattering

The experimental Compton profiles of aluminum and nickel were corrected for double scattering. The Al profiles were obtained from our previous measurements[3] performed using 60-keV γ rays from an ^{241}Am source. The results are given in Table III. The profiles have been normalized so that the area under the high energy side of the profiles between $p_z = 0.0$ and $p_z = 7.0$ a.u. is equal to 6.16, the theoretical free-atom area. The Compton profiles are not altered from our previous results[3] and, indeed, the extension of our Monte Carlo method does not affect the corrections made for relatively thin samples and samples of low absorption. This is due to the fact that the scattering angles of a double-scattering process are bound to be so high that the elastic scattering contributes only a small proportion to the total intensity and then the approximation used previously ($f_R^2 + f_c \simeq Z$) is valid. For thicker samples, the proper inclusion of elastic scattering gives rise to the increase in double-scattered intensity, since there is then a higher probability of small-angle scattering in the sample and f_R^2 approaches Z^2. In Table III we have also given the theoretical Compton profiles calculated by Cooper *et al.*[15] and Kubo *et al.*[16] The theoretical profiles of Table III do not include the resolution effects of our experiment. By convoluting the theoretical profiles with the residual instrumental function excellent agreement is obtained between theory and experiment.[3,16] The experimental Compton profiles of nickel were obtained from the measurements of Manninen and Paakkari[17] and Eisenberger *et al.*[18] measured at Am and Te energies, respectively. The latter measurement gives a good check for relativistic calculations, since at that energy the relativistic effects will be significant. The results are given in Table IV. The normalization constants are 12.17 and 12.25 for Am and Te radiation, respectively. At Am en-

TABLE IV. Compton profile of nickel. Am and Te refer to the experimental profiles measured using Am and Te radiation, respectively. The sample thicknesses were 0.291 and 0.0584 cm, the radii of the cylindrical samples were 0.6 and 0.95 cm and the scattering angles were 165° and 173°, respectively. The areas of the theoretical profiles do not include the $1s^2$ contribution beyond 4.0 a.u.

p_z	Theory[a]	Theory[b]	No correction for MS		Corrected for MS	
			Am[c]	Te[d]	Am[c]	Te[d]
0.0	5.259	5.38	5.086 ± 0.4%	5.159 ± 1.0%	5.258 ± 0.4%	5.325 ± 1.0%
0.1	5.238	5.37	5.075	5.139	5.239	5.302
0.2	5.170	5.31	5.027	5.093	5.186	5.253
0.3	5.068	5.23	4.943	5.017	5.096	5.174
0.4	4.919	5.10	4.827	4.907	4.971	5.055
0.5	4.725	4.93	4.684	4.752	4.818	4.892
0.6	4.487	4.70	4.519	4.566	4.639	4.692
0.7	4.200	4.48	4.340	4.363	4.447	4.472
0.8	3.897	4.30	4.154	4.156	4.246	4.249
0.9	3.773	4.14	3.969	3.961	4.049	4.039
1.0	3.687	3.95	3.787 ± 0.5%	3.801 ± 2.0%	3.854 ± 0.5%	3.868 ± 2.0%
1.2	3.471	3.60	3.448	3.466	3.494	3.511
1.4	3.226	3.25	3.153	3.167	3.182	3.193
1.6	2.962	2.92	2.885	2.887	2.899	2.896
1.8	2.693	2.61	2.624	2.617	2.622	2.612
2.0	2.430	2.29	2.365 ± 0.6%	2.355 ± 5.0%	2.349 ± 0.6%	2.339 ± 5.0%
2.2		2.03	2.117	2.107	2.089	2.083
2.4		1.83	1.896	1.908	1.861	1.877
2.6		1.63	1.715	1.772	1.677	1.742
2.8		1.47	1.555	1.535	1.518	1.494
3.0	1.402	1.30	1.411	1.377	1.374	1.333
3.5	1.082	0.97	1.117	1.073	1.076	1.030
4.0	0.872	0.78	0.887 ± 0.9%	0.859 ± 7.0%	0.849 ± 0.9%	0.821 ± 7.0%
4.5		0.57	0.688	0.706	0.653	0.672
5.0	0.547	0.48	0.571	0.598	0.542	0.569
6.0	0.395		0.414	0.445	0.392	0.425
7.0			0.303 ± 1.5%	0.340	0.291	0.325

[a]Reference 19. [b]Reference 20.
[c]Reference 17. [d]Reference 18.

ergy, the theoretical area does not include $1s^2$ contribution in the momentum region from 4.2 to 7.0 a.u., since the 1s electrons cannot then be excited. The agreement between the two experimental profiles after correcting for double scattering is fairly good throughout the range of p_z from 0.0 to 4.0 a.u. that can be used for comparison. In Table IV we have presented the theoretical Compton profiles of nickel calculated using a RFA (renormalized free atom) model[19] and a self-consistent–linear-combination-of-atomic-orbitals (SC-LCAO) model.[20] Agreement with theory is much improved after correction for multiple scattering. In Fig. 5 we have given the spectral distribution of double scattering for nickel at Am and Te energies with the corresponding single profiles normalized according to Eq. (24). The normalization constants are 28.6 and 28.1 for Am and Te radiation, respectively. It is seen that the width of the double-scattered profile relative to the single-scattered profile is the same at both energies. However, the spectral distribution of double scattering at 160 keV is more symmetric and centered at the peak of the single profile. In the case of Ni samples the ratios of double-to-single scattering were 9.3% (Am) and 11.4% (Te) giving rise to a correction of 3.4% and 3.1% at $J(0)$.

In order to check the effects of Ribberfors correction terms in Eq. (18) we calculated the spectral distributions including only the classical term; i.e., the last term of Eq. (18). As expected from the results of Williams[21] no significant difference was found between the nonrelativistic and relativistic results and this gives us justification to drop the first three terms of the square brackets in Eq. (18) in order to reduce the computing time.

D. Comparison with other work

Tanner and Epstein[7,8] have undertaken a thorough analytic and Monte Carlo investigation of single-

and double-scattered intensities in cylindrical samples. Their approach is rather general and by the introduction of a simplified model of the experimental situation they are able to deduce the effects of different cross sections on the intensities and the spectral distributions of double scattering. Their results are in qualitative agreement with the results of this paper, indicating that at the energies less than 160 keV the differences between the polarized averaged Klein-Nishina and Thomson cross sections are not marked. However, because no application to experimental Compton profiles was carried out it is difficult to make detailed comparison with their results. The recent results of Braun-Keller and Epstein[22,23] give more insight into the possibility of finding an operational tool for correcting for the effects of multiple scattering in Compton profile measurements.

Paatero and Halonen[14] have derived analytic functions which can be used to estimate the amount of double scattering in certain experimental situations. Using the results of their paper the ratios of double-to-single scattering for nickel at 180° scattering angle and with optical thickness $\mu d = 0.1$, are 0.1%, 1.5%, and 14.4% for Mo$K\alpha$, Am and Te energy, respectively. We can see from Fig. 3 that those results are very close to the values obtained here.

The method of Felsteiner *et al.*[5,6] has been discussed in earlier papers. In their last paper[24] they include the electron binding which was a serious drawback in their earlier version. Their results for titanium[24] are now in very good agreement with those of Manninen and Paakkari[25] corrected for double scattering using our Monte Carlo program.

IV. CONCLUSIONS

Using our recent extended version of the Monte Carlo method of correcting for the effects of multiple scattering we have shown that the magnitude of the relativistic and nonrelativistic cross sections is quite different at an energy of 160 keV, but that the energy dependence of the two cross sections is essentially the same. Furthermore, we have shown that in the cases of interest, the relativistic Klein-Nishina and Ribberfors cross sections do not differ significantly as far as these are concerned, and one can use the Klein-Nishina formula in order to make the calculations more efficient. Finally, the validity of this work has been assessed by correcting a number of experimental profiles for double scattering. Comparisons between different experimental profiles as well as between experimental and theoretical profiles all indicate the reliability of the results discussed above.

ACKNOWLEDGMENTS

We would like to thank Dr. T. Paakkari, Dr. S. Manninen, and Dr. P. Pattison for most valuable discussions regarding various aspects of the problems in Compton scattering.

[1] For a review, see V. Halonen, I. R. Epstein, A. C. Tanner, and B. G. Williams, in *Compton Scattering: The Investigation of Electron Momentum Distributions*, edited by B. G. Williams (McGraw-Hill, London, 1977).
[2] B. G. Williams and V. Halonen, Phys. Fenn. 10, 5 (1975).
[3] V. Halonen, B. G. Williams, and T. Paakkari, Phys. Fenn. 10, 107 (1975).
[4] V. Halonen, thesis (University of Helsinki, 1975) (unpublished).
[5] J. Felsteiner, P. Pattison, and M. J. Copper, Philos. Mag. 30, 537 (1974).
[6] J. Felsteiner and P. Pattison, Nucl. Instrum. Methods 124, 449 (1975).
[7] A. C. Tanner and I. R. Epstein, Phys. Rev. A 14, 313 (1976).
[8] A. C. Tanner and I. R. Epstein, Phys. Rev. A 14, 328 (1976).
[9] R. Ribberfors, Phys. Rev. B 12, 2067 (1975).
[10] R. Ribberfors, Phys. Rev. B 12, 3136 (1975).
[11] T. Paakkari and V. Halonen (unpublished).
[12] *International Tables for X-Ray Crystallography* IV (Kynoch, Birmingham, 1974).
[13] P. A. Doyle and P. S. Turner, Acta Crystallogr. A 24, 391 (1968).
[14] P. Paatero and V. Halonen, Nucl. Instrum. Methods 135, 537 (1976).
[15] M. J. Cooper, P. Pattison, B. G. Williams, and K. C. Pandey, Philos. Mag. 29, 1237 (1974).
[16] Y. Kubo, S. Wakoh, and J. Yamashita, J. Phys. Soc. Jpn. 41, 836 (1976).
[17] S. Manninen and T. Paakkari (private communication, 1977).
[18] P. Eisenberger and W. A. Reed, Phys. Rev. B 9, 3242 (1974).
[19] T. Paakkari, S. Manninen, and K. F. Berggren, Phys. Fenn. 10, 207 (1975).
[20] Numerical values of Dr. Wang are given for nickel in Ref. 19.
[21] B. G. Williams, Acta. Crystallogr. A 32, 513 (1976).
[22] E. Braun-Keller and I. R. Epstein (unpublished).
[23] E. Braun-Keller and I. R. Epstein (unpublished).
[24] J. Felsteiner and P. Pattison, Phys. Rev. B 13, 2702 (1976).
[25] S. Manninen and T. Paakkari, J. Phys. C 9, 95 (1976).